XLII Summer School
ADVANCED PROBLEMS IN MECHANICS
Repino, St. Petersburg, Russia 2014

Numerical simulation of local field concentration near the contour of a fracture

Dawid Jaworski, Alexander Linkov, Ewa Rejwer,
Liliana Rybarska-Rusinek

Rzeszow University of Technology, Poland

The support of the EU Marie Curie IAPP transfer of knowledge programme is gratefully acknowledged

HYDROFRAC; grant #251475

Motivation

Hydraulic fracturing is commonly performed
in the rock composed of layers, structural blocks
and containing inhomogeneities like inclusions, pores and cracks.

Our objective is to develop computational techniques applicable to efficient evaluation of local fields in strongly inhomogeneous media with multiple cracks, pores and inclusions

We use the **H-BIE**, tailored for blocky structures, which take into account discontinuities and singularities of fields

Problems to be discussed

- **2D problems**: employing the complex variable (CV) fast multipole method combined with the boundary element method, based on the CV hypersingular boundary integral equation
- **3D problems**: employing 3D hypersingular boundary integral equation in frames of the boundary element method

Solving 2D problems employing the complex variable hypersingular boundary integral equations

Part 1.

2D problems

Solving 2D problems employing the complex variable hypersingular boundary integral equations

- Basic complex variable integrals
- Approximation of the contour and the density function
- The CV fast multipole boundary element method
- Numerical example

Basic complex variable integrals

Solving the CV H-BIE it is sufficient to focus on two integrals, **singular (S) and hypersingular (H):**

$$S = \int_{L_e} \frac{f(\tau)}{\tau - t} d\tau, \quad H = \int_{L_e} \frac{f(\tau)}{(\tau - t)^2} d\tau,$$

where L_e is the boundary element, $f(\tau)$ is the density function, $t = x + iy$ and τ are the CV coordinates of the field point and integration point, respectively.

A.M. Linkov. Boundary integral equations in elasticity theory. Kluwer Academic Publishers, Dordrecht-Boston-London, 2002.
Ewa Rejwer, Liliana Rybarska-Rusinek, Aleksandr Linkov. The complex variable fast multipole boundary element method for the analysis of strongly inhomogeneous media. Engineering Analysis with Boundary Elements 43 (2014): 105-116.

Smooth approximation of the contour by the straight and circular-arc boundary elements

Linear transformation of coordinates from global to local system:

$$\tau = \tau_c + A \exp(i\alpha_c)\tau',$$

a) straight element ($A = l$)

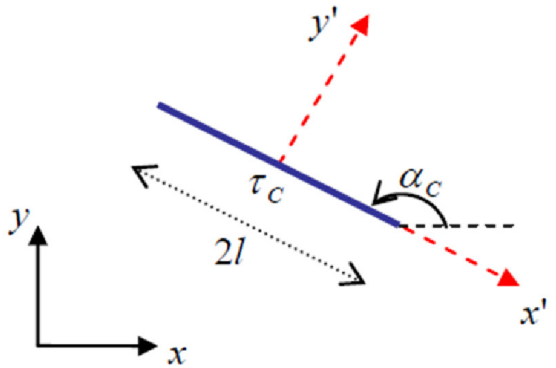

b) circular-arc element ($A = -iR$)

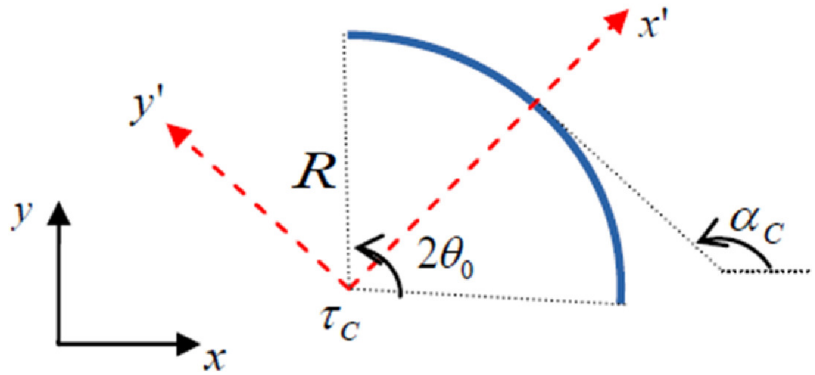

The straight and the circular-arc elements are transformed into **the standard forms**, of **unit half length** ($l = 1$) and **unit radius** ($R = 1$), respectively

Approximation of the density function

General approximation of the density function, for both ordinary and singular elements, is:

$$f(\tau) = (\tau - c)^{\beta} P(\tau),$$

where c is the end point of the integration path;
$P(\tau)$ is a linear combination of the form functions;

- for an ordinary (non-tip) element $\beta = 0$,
- for a singular (tip, multi-wedge) element $\beta = \frac{m}{n}$, $|\beta| < 1$;
  e.g. for the displacement discontinuity and traction near a crack tip, $\beta = 1/2$ and $\beta = -1/2$, respectively.

Approximation of the density function

General approximation of the density function, for both ordinary and singular elements, is:

$$f(\tau) = (\tau - c)^{\beta} P(\tau),$$

where c is the end point of the integration path;
$P(\tau)$ is a linear combination of the form functions;

- for an ordinary (non-tip) element $\beta = 0$,
- for a singular (tip, multi-wedge) element $\beta = \frac{m}{n}$, $|\beta| < 1$;
  e.g. for the displacement discontinuity and traction near a crack tip, $\beta = 1/2$ and $\beta = -1/2$, respectively.

The value of β for singular multi-wedge elements, is found by the standard procedure.

Blinova V.G., Linkov A.M., *A method to find asymptotic forms at the common apex of elastic wedges.*, J. Appl. Math. Mech., 1995, 59 (2), 187-195.
Linkov A.M., Koshelev V.F., *Muti-wedge points and multi-wedge elements in computational mechanics: evaluation of exponent and angular distribution*, Int. J. Solids and Structures, 2006, 43, 5909-5930.

The CV fast multipole boundary element method

Considering strongly inhomogeneous structures demands the analysis of problems with hundred of thousends of DOF.
The efficient approach to deal with such problems, is to combine the BEM with the fast multipole method (FMM).

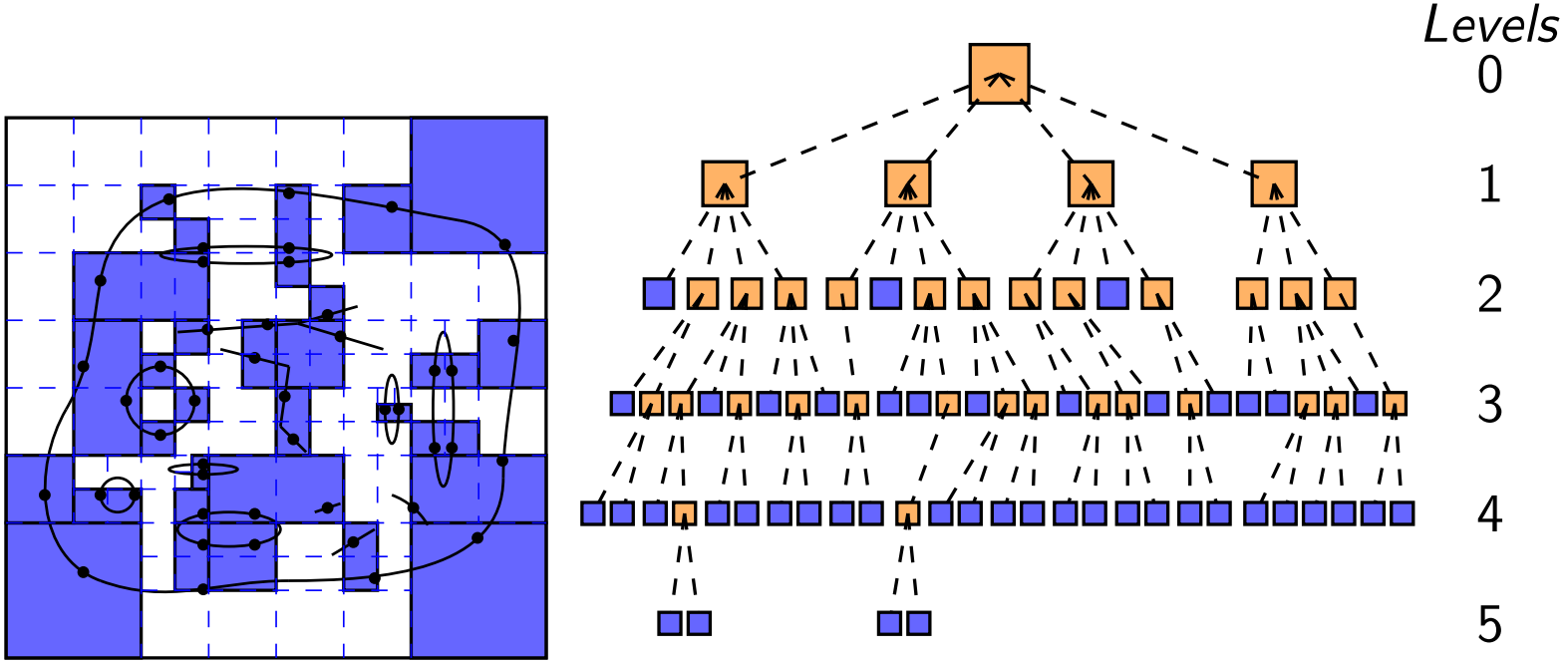

Hierarchical quad-tree structure employed in the FMM

Y.J. Liu. Fast multipole boundary element method: theory and applications in engineering. Cambridge University Press, 2009.

The CV fast multipole boundary element method

Considering strongly inhomogeneous structures demands the analysis of problems with hundred of thousends of DOF.
The efficient approach to deal with such problems, is to combine the BEM with the fast multipole method (FMM).

The method suggested is free from numerical integration: all integrals in frames of BEM and FMM are evaluated analytically employing recurrent formulae.

Comprehensive presentation of all details may be found at:

Ewa Rejwer, Liliana Rybarska-Rusinek, Aleksandr Linkov. The complex variable fast multipole boundary element method for the analysis of strongly inhomogeneous media. Engineering Analysis with Boundary Elements 43 (2014): 105-116.

Numerical applications

The method developed may be applied for

- finding the effective properties of an inhomogeneous material (total flux, effective conductivity, effective moduli);
- evaluating a local concentration of fields (FIFs, SIFs).

Here we present one numerical example:
evaluation of the local fields to characterize the strength of a material, by employing the statistics of extremes.

Numerical example

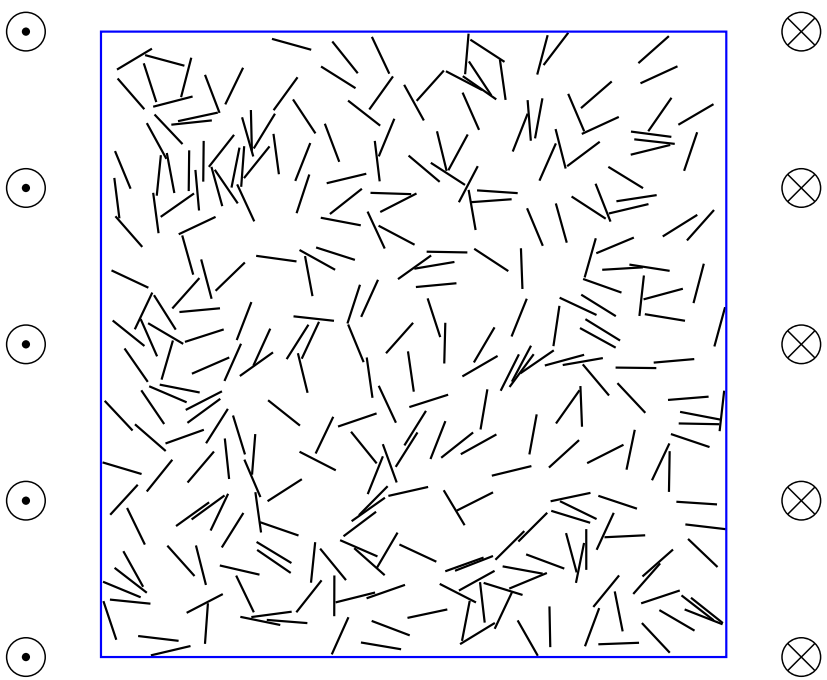

Consider antiplane shear of a cell with randomly distributed cracks (non-intersecting and intersecting) of equal half-length l and the crack density

$$\rho = \frac{N_c l^2}{A},$$

where A is the area of the cell, N_c is the number of cracks in it. The crack angle is uniformly distributed in the interval $[0, \pi]$.

Numerical example

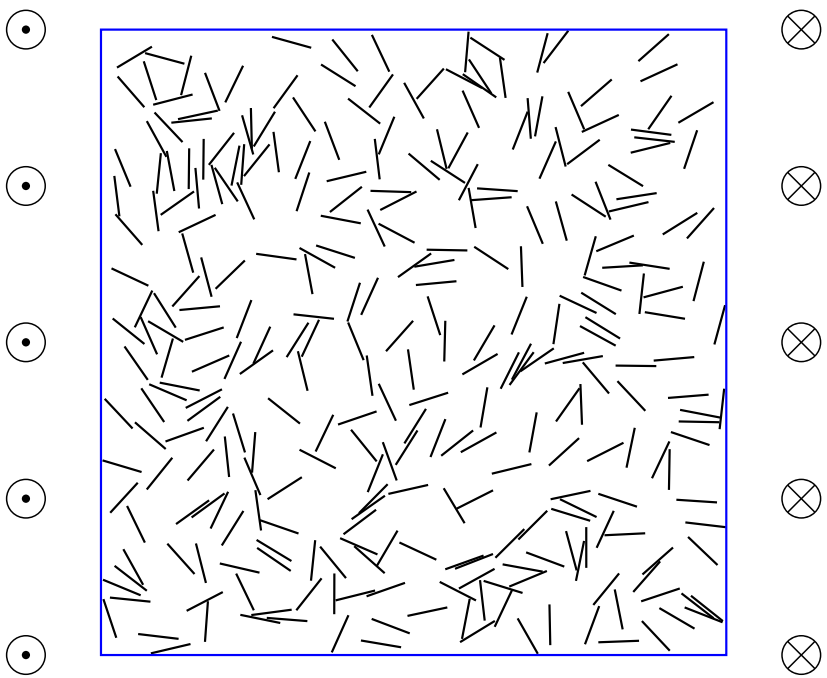

Consider antiplane shear of a cell with randomly distributed cracks (non-intersecting and intersecting) of equal half-length l and the crack density

$$\rho = \frac{N_c l^2}{A},$$

where A is the area of the cell, N_c is the number of cracks in it. The crack angle is uniformly distributed in the interval $[0, \pi]$.

Each side of the RVE is represented by equal number of ordinary **straight boundary elements**. Each crack by four straight elements: **two ordinary and two tip**.

Boundary conditions

We assume the following boundary conditions:

- zero tractions at the crack surfaces;
- constant displacements $u_l = 0$ and $u_r = u^0$ at the left and right vertical sides of the cell, respectively;
- zero shear traction $\sigma^0_{zy} = 0$ at the horizontal sides of the cell.

Boundary conditions

We assume the following boundary conditions:

- zero tractions at the crack surfaces;
- constant displacements $u_l = 0$ and $u_r = u^0$ at the left and right vertical sides of the cell, respectively;
- zero shear traction $\sigma^0_{zy} = 0$ at the horizontal sides of the cell.

The difference in the values of shear stress σ^0_{xz}, calculated on the left and right side of the cell, gives an integral estimation of the computational error

In the calculations, the relative error of σ^0_{xz} does not exceed 0.52%.

Calculation of a stress intensity factor

Distribution of the SIF K_{III} is studied by employing the CV FM-BEM, which allows solving problems for the cell with large number of non-intersecting and/or intersecting cracks.

Calculation of a stress intensity factor

Distribution of the SIF K_{III} is studied by employing the CV FM-BEM, which allows solving problems for the cell with large number of non-intersecting and/or intersecting cracks.

In the calculations we increased the number N_c from 100 to 300 for the crack density $\rho = 0.32$.

Increasing the number of seeded cracks led to too many configurations with almost parallel closely located cracks. **Decreasing distance between cracks, the condition number of the system tends to infinity.**

Stress intensity factor at the crack tips

Figures present a distribution of 300 non-intersecting and intersecting cracks. Unfilled (dark) circle near a crack tip shows the magnitude of a positive (negative) SIF. The radius of a circle is proportional to the SIF.

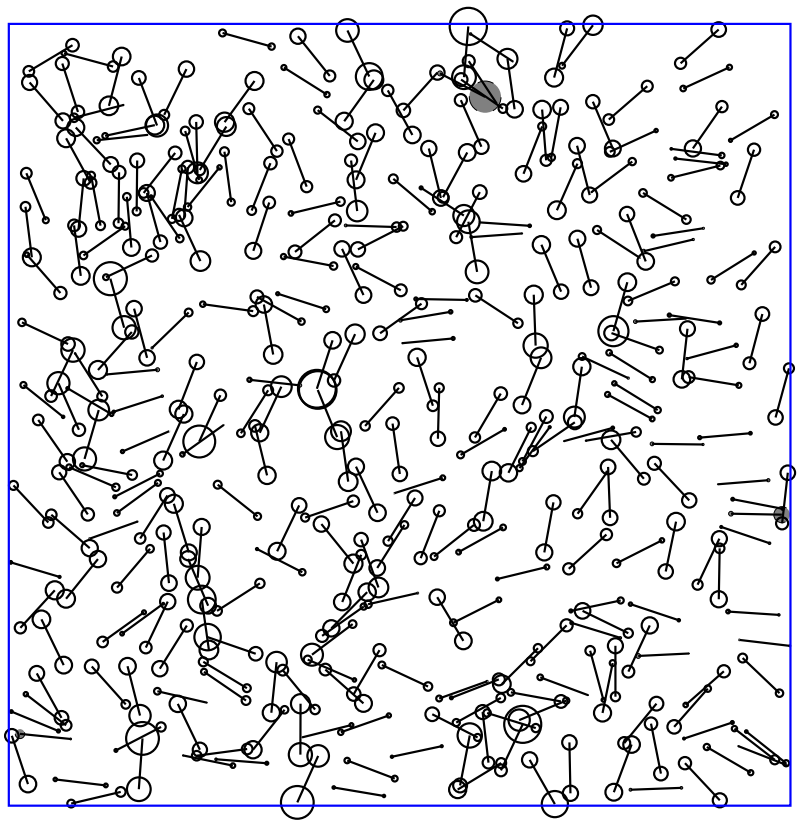

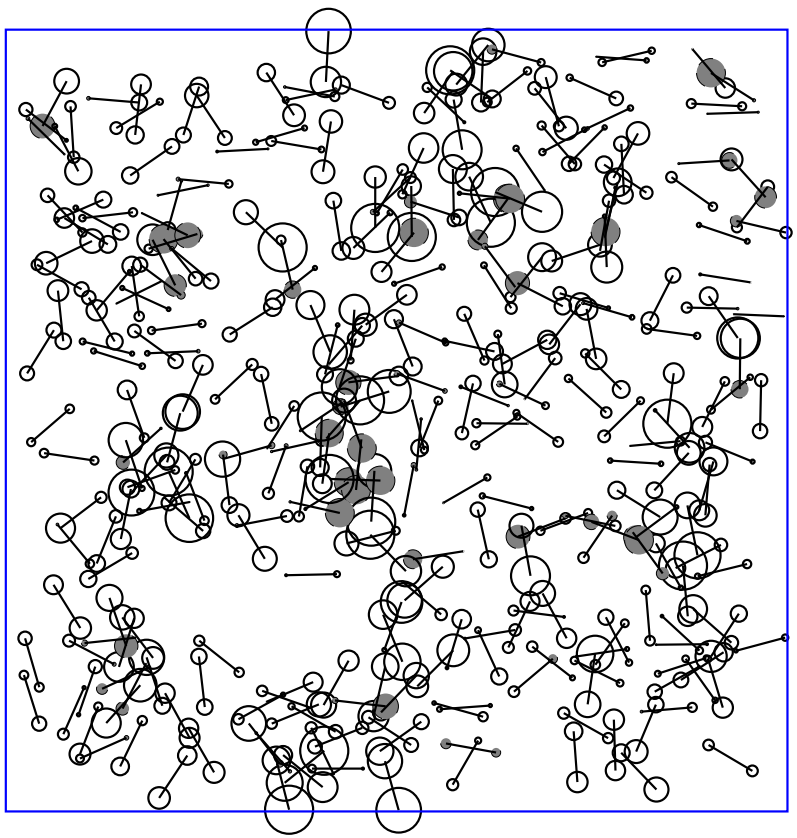

Stress intensity factor distribution for $\rho = 0.32$

The empirical cumulative probability function for the density 0.32, for non-intersecting and intersecting cracks.

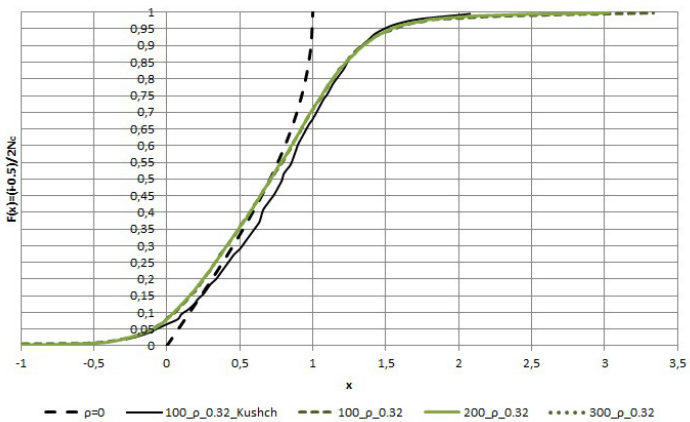

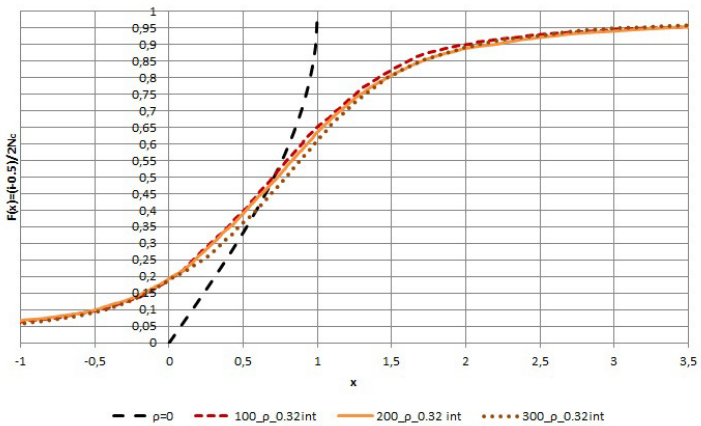

Stress intensity factor distribution for $\rho = 0.32$

The empirical cumulative probability function for the density 0.32, for non-intersecting and intersecting cracks.

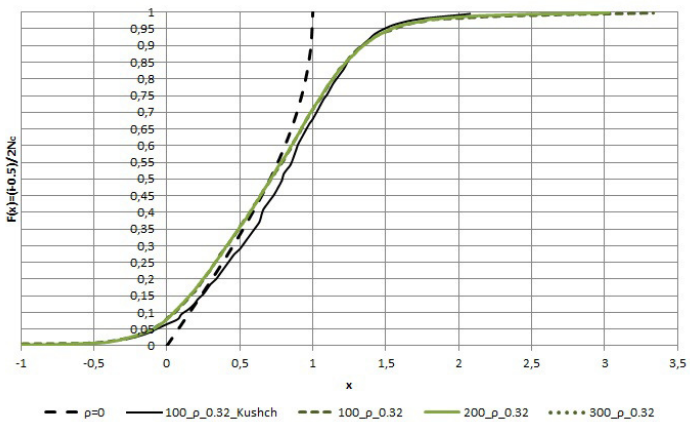

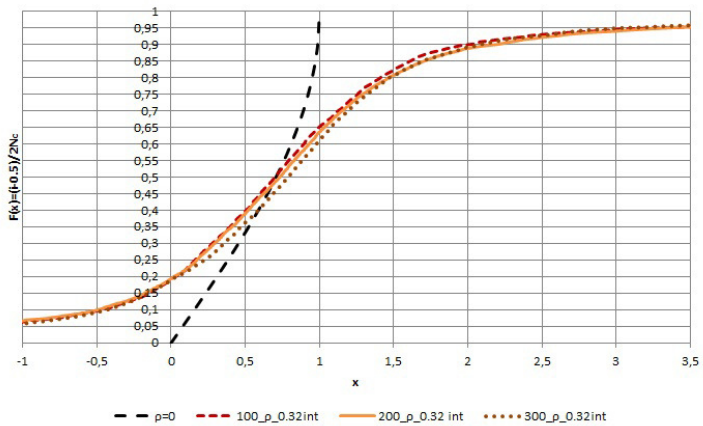

To overcome the computational difficulty, for the crack density 0.32, we were repeating random seeding of 100, 200 and 300 cracks in 50, 24 and 16 tests, respectively. In the statistical sense the averaged results of those tests correspond to seeding 5000, 4800 and 4800 cracks in a single cell.

Stress intensity factor distribution for $\rho = 0.32$

The empirical cumulative probability function for the density 0.32, for non-intersecting and intersecting cracks.

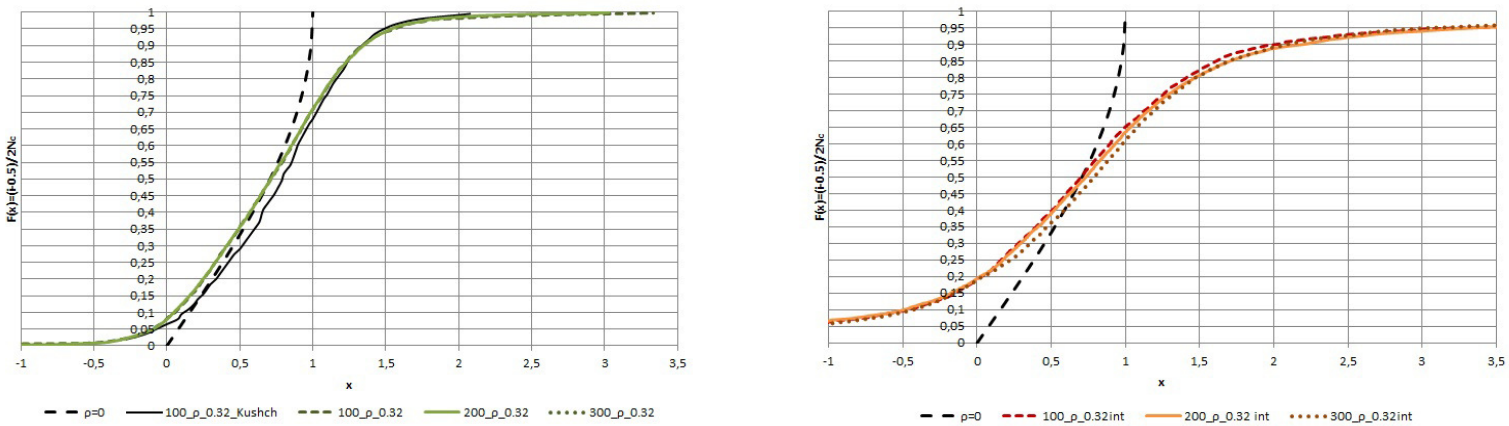

Dark dashed curve corresponds to zero density.

The results for non-intersecting cracks, which has been studied by another method in the paper by Kushch, are presented by a solid dark curve. The results are comparable. For the tail, they are practically the same.

e.g. V.I. Kushch, S.V. Shmegera, I. Sevostianov. SIF statistics in micro cracked solid: Effect of crack density, orientation and clustering. Int. J. Eng. Sci., 47: 192-208, 2009.

Stress intensity factor distribution for $\rho = 0.32$

The empirical cumulative probability function for the density 0.32, for non-intersecting and intersecting cracks.

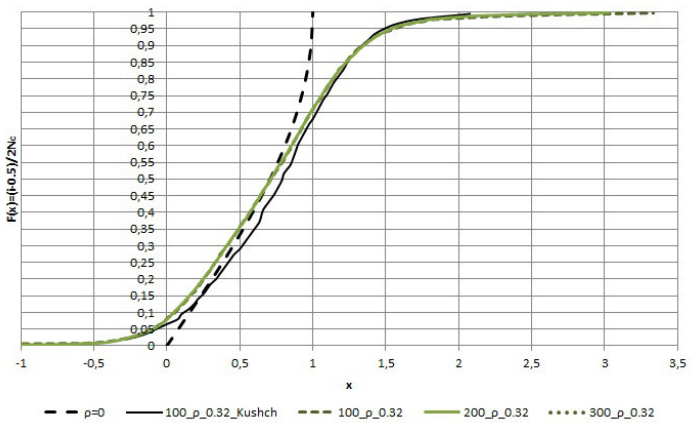

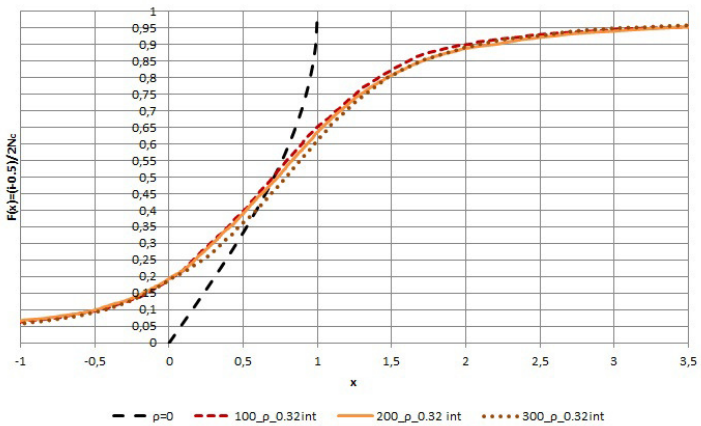

For intersecting cracks there appear notable portion of cracks with very high values of the SIF, so that the tails extend much farer.

Approximation of the distribution function

The statistical analysis is performed using the Extreme Value Theory.
Analysis shows that, for the **non-intersecting cracks**, the tail of the empirical cumulative probability function $F(x)$ is fitted well by the Weibull type Generalized Extreme Value (GEV) distribution:

$$F(x) = exp\left(-\left(1 + k\frac{x-\mu_p}{\sigma_p}\right)^{-\frac{1}{k}}\right),$$

where $k < 0$. The parameters of distribution are about:
$k = -0.25$, $\mu_p = 0.53$, $\sigma_p = 0.49$.

Approximation of the distribution function

The statistical analysis is performed using the Extreme Value Theory.
Analysis shows that, for the **non-intersecting cracks**, the tail of the empirical cumulative probability function $F(x)$ is fitted well by the Weibull type Generalized Extreme Value (GEV) distribution:

$$F(x) = exp\left(-\left(1 + k\frac{x-\mu_p}{\sigma_p}\right)^{-\frac{1}{k}}\right),$$

where $k < 0$. The parameters of distribution are about:
$k = -0.25$, $\mu_p = 0.53$, $\sigma_p = 0.49$.

For **intersecting cracks**, the tail of the function $F(x)$, is fitted well by the Gumbel type GEV distribution:

$$F(x) = exp\left(-exp\left(-\frac{x-\mu_p}{\sigma_p}\right)\right).$$

The parameters of the distribution, are about: $\mu_p = 0.35$, $\sigma_p = 0.83$.

Statistics of the stress intensity factor distribution for $\rho = 0.06$

For lower densities the number of cracks in the cell may be increased and the tests decreased. For the density $\rho = 0.06$, for non-intersecting cracks, we take: $N_t = 50$, 20, 5, 3 tests, for $N_c = 100$, 500, 1000, 1500; for intersecting cracks, we take: $N_t = 50$, 10, 7 tests, for $N_c = 100$, 500, 700 cracks.

Statistics of the stress intensity factor distribution for $\rho = 0.06$

For lower densities the number of cracks in the cell may be increased and the tests decreased. For the density $\rho = 0.06$, for non-intersecting cracks, we take: $N_t = 50$, 20, 5, 3 tests, for $N_c = 100$, 500, 1000, 1500; for intersecting cracks, we take: $N_t = 50$, 10, 7 tests, for $N_c = 100$, 500, 700 cracks.

The empirical cumulative probability function for non-intersecting and intersecting cracks with the density $\rho = 0.06$ is presented below.

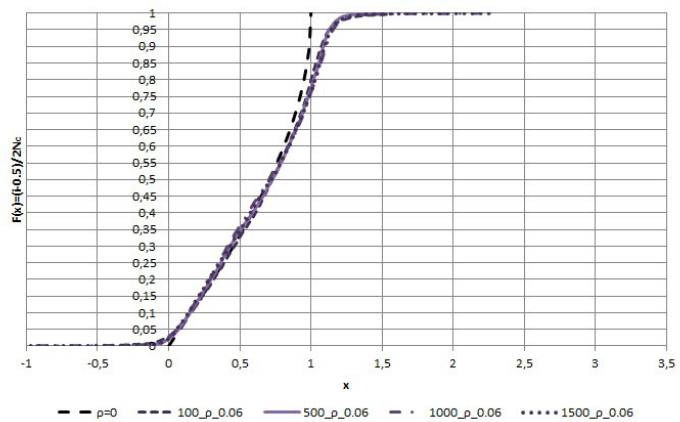

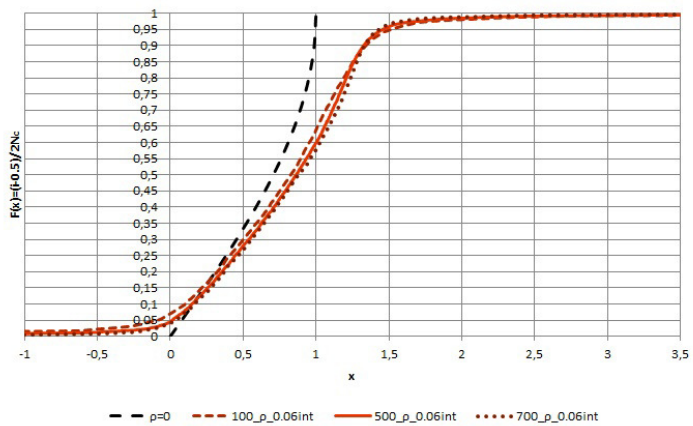

Statistics of the stress intensity factor distribution for $\rho = 0.06$

**The figure shows that the distributions practically coincide.
This confirms that for low densities ($\rho \leqslant 0.06$),
the number of seeded cracks may be taken greater,
while the number of tests less than for high densities ($\rho \geqslant 0.24$).**

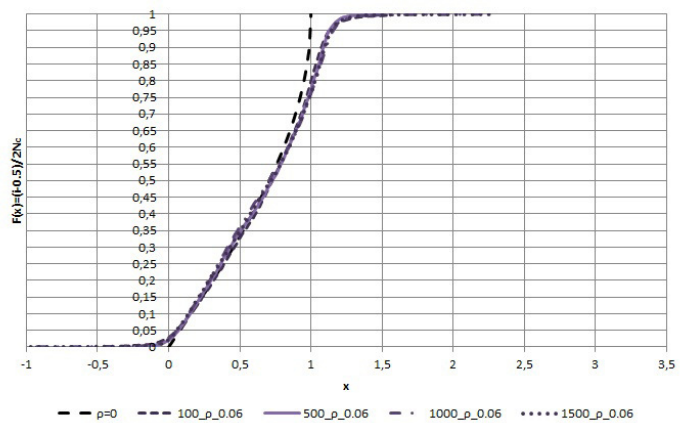

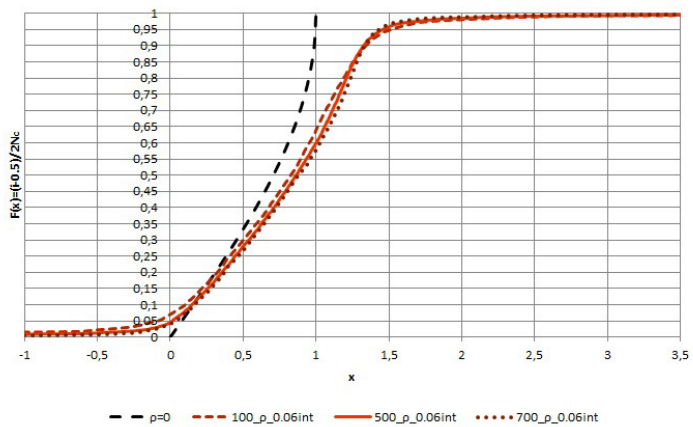

Calculation of a fracture risk

The data on extreme values provide us with the measure of fracture risk of a microfractured solid.

The maximal load is defined by the condition:

$$F(K_s) = P(K'_{III} < K_s) = 1 - \delta,$$

where $K_s = \sigma^c_{xz}/\sigma^0_{xz}$ corresponds to the accepted probability δ of fracture; σ^c_{xz} is the critical SIF, found in tests.

Calculation of a fracture risk

The data on extreme values provide us with the measure of fracture risk of a microfractured solid.

The maximal load is defined by the condition:

$$F(K_s) = P(K'_{III} < K_s) = 1 - \delta,$$

where $K_s = \sigma^c_{xz}/\sigma^0_{xz}$ corresponds to the accepted probability δ of fracture; σ^c_{xz} is the critical SIF, found in tests.

The values of K_s ("safety factor"), corresponding to the level $\delta = 0.05$ of fracture risk, for crack densities 0.0, 0.06 and 0.32, are given in the Table.

Crack configuration	$\rho = 0.0$	$\rho = 0.06$	$\rho = 0.32$
non-intersected	0.9969	1.1282	1.5709
intersected	0.9969	1.5133	3.0764

Conclusions from numerical example

- the CV fast multipole BEM may be applied for studying the extreme values of the SIFs at tips of both non-intersecting and intersecting, randomly seeded cracks;
- for the density exceeding 0.24, when the number of cracks in a cell exceeds 300, it is reasonable to seed acceptable number of cracks and to repeat statistical tests, rather than to take excessively large number of cracks in a representative cell;
- for the crack density 0.32, using the CV fast multipole BEM reduces the number of statistical tests three-fold, at least, as compared with a BEM not combined with the fast multipole method.

Solving 3D problems employing the hypersingular boundary integral equations

Part 2.

3D problems

Solving 3D problems employing the hypersingular boundary integral equations

- Integrals entering hypersingular boundary integral equation (H-BIE)
- Approximation of the surface and the density function
- Numerical example

Integrals entering H-BIE

Inspection of the BIE of static 3D potential and elasticity theory shows that it is sufficient to consider the function

$$\int_{S^q} \frac{f(y)}{R} dS_y,$$

and its spatial derivatives: $\partial/\partial x_i$, $\partial^2/\partial x_i \partial x_j$, $\partial^3/\partial x_i \partial x_j \partial x_k$.

Herein, S^q is the surface of a boundary element; $f(y)$ is a function (density) to be properly approximated on the element and R is the distance between the field and integration points.

Linkov, A. M., V. V. Zubkov, and M. A. Kheib. *A method of solving three-dimensional problems of seam workings and geological faults*. Journal of Mining Science 33.4 (1997): 295-315.
Linkov A. M., *Boundary Integral Equations in Elasticity Theory*, Dordrecht-Boston-London, Kluwer Academic Publishers, 2002, 268 p.

Approximation of the surface by the trapezoidal elements

We solve the H-BIE by **the boundary element method** and represent the surface by the sum of ordinary and edge trapezoidal elements S^q (commonly used triangular, square and rectangular elements are their special cases).

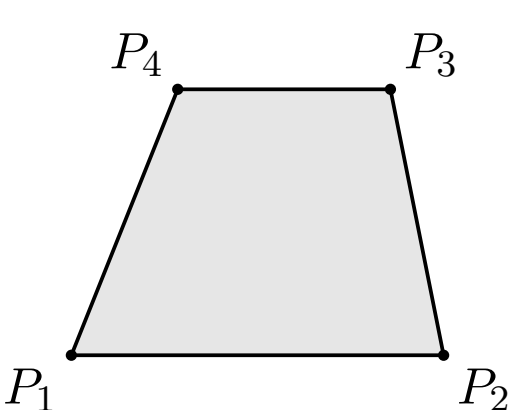

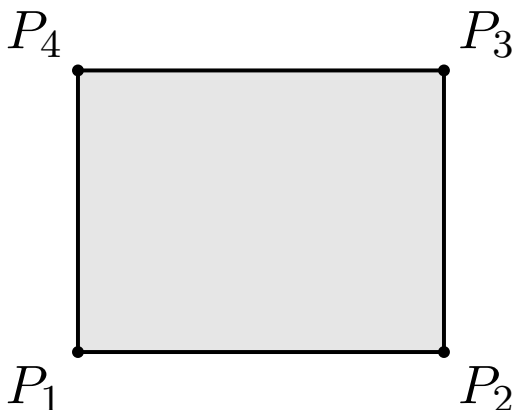

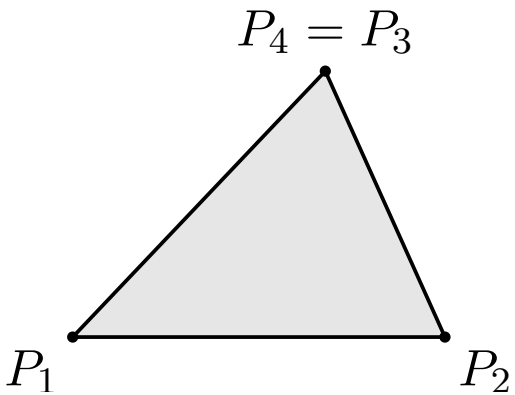

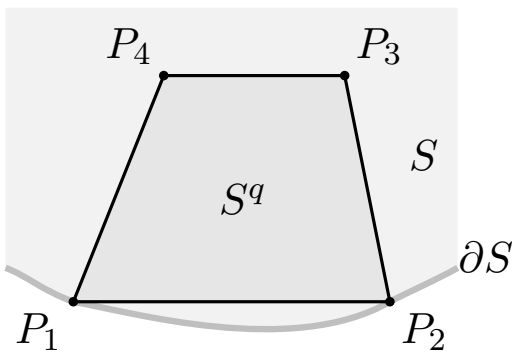

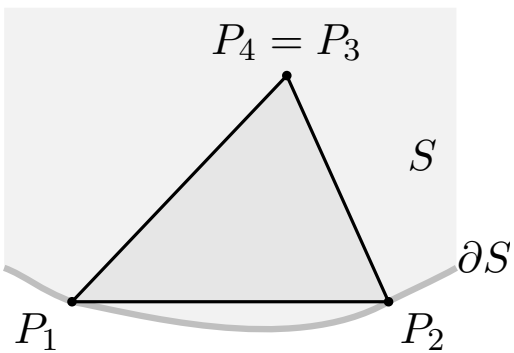

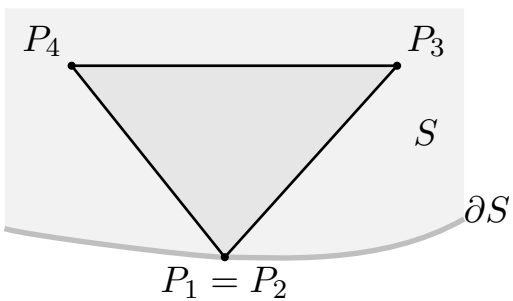

Mesh of a spherical cap-crack

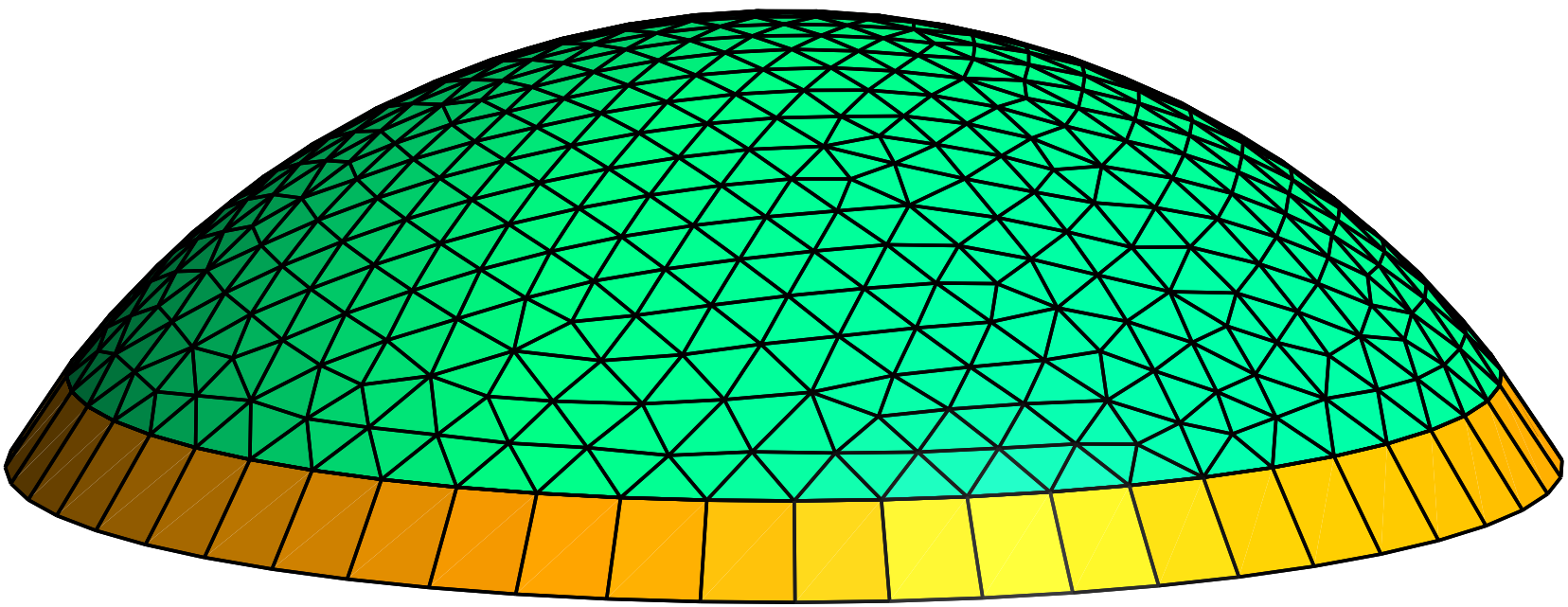

Mesh of a spherical cap-crack

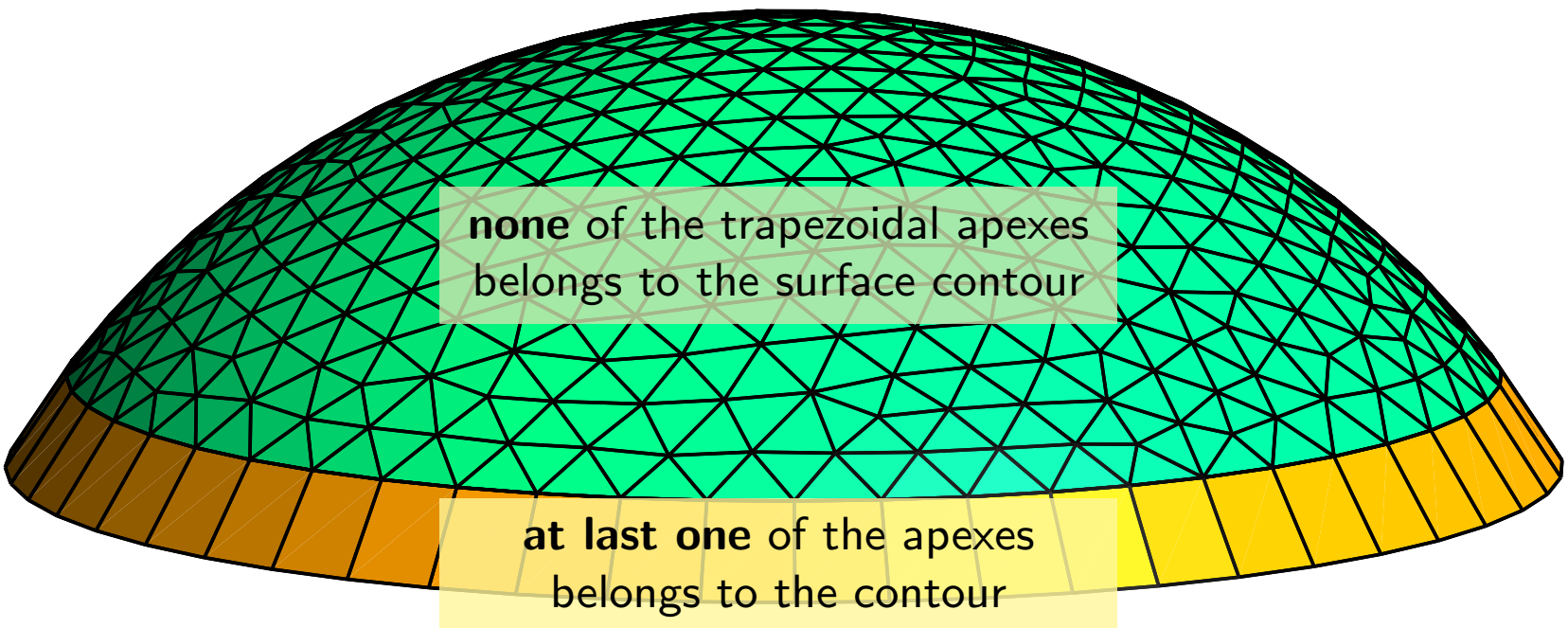

Approximation of density

The integration is performed in the local coordinate system of each element. We approximate the density function as follows:

$$f(y) = y_3^{\alpha} \sum_{k+l=0}^{m_p} c_{kl} y_2^k y_3^l, \qquad 0 \leqslant \alpha < 1,$$

where m_p is the degree of a polynomial approximating the density and c_{kl} are coefficients of the approximation.

Liliana Rybarska-Rusinek, Dawid Jaworski, Aleksandr Linkov *On efficient evaluation of integrals entering boundary equations of 3D potential and elasticity theory*, Journal of Mathematics and Applications JMA No 37, (2014) (in print)

Approximation of density

The integration is performed in the local coordinate system of each element. We approximate the density function as follows:

$$f(y) = y_3^{\alpha} \sum_{k+l=0}^{m_p} c_{kl} y_2^k y_3^l, \qquad 0 \leqslant \alpha < 1,$$

where m_p is the degree of a polynomial approximating the density and c_{kl} are coefficients of the approximation.

For $\alpha = 0$ and $\alpha = 1/2$ all integrals may be evaluated recurrently. Starting integrals are evaluated analytically ($\alpha = 0$) or by using Carlson algorithms for elliptic integrals ($\alpha = 1/2$).

Liliana Rybarska-Rusinek, Dawid Jaworski, Aleksandr Linkov *On efficient evaluation of integrals entering boundary equations of 3D potential and elasticity theory*, Journal of Mathematics and Applications JMA No 37, (2014) (in print)

Example: the penny-shaped crack in an infinite medium

We consider the 3-D problem of a single planar crack in an infinite isotropic linear elastic medium subjected to either normal or shear far-field stresses.

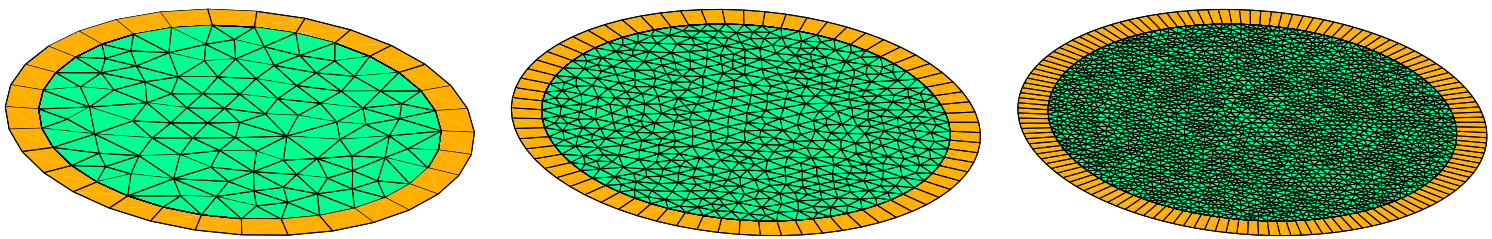

We approximate the crack by $N = 18$ $(220, 1010, 3932)$ elements. The internal, ordinary elements are triangles, edge elements are trapezoids with different height ($h = h^{\triangle}$, $h = 2h^{\triangle}$, $h = 4h^{\triangle}$).

Case 1: penny-shaped crack under normal far-field stresses

N	$h/h^{\triangle}$	Constant approximation δK_1^{rel}	δu^{max}	δu^{rms}	Square root appr. δK_1^{rel}	δu^{max}	δu^{rms}
18	1	0.1364	0.2230	0.1697	0.0790	0.1740	0.1317
	2	0.1494	0.2670	0.2015	0.0388	0.1576	0.1296
220	1	0.2034	0.2489	0.1014	0.0786	0.1125	0.0550
	2	0.1870	0.2304	0.0947	0.0404	0.0791	0.0494
1010	1	0.2081	0.2473	0.0697	0.0701	0.0892	0.0350
	2	0.1793	0.2078	0.0577	0.0342	0.0543	0.0267
3932	1	0.2237	0.2444	0.0496	0.0650	0.0827	0.0235
	2	0.1757	0.1897	0.0380	0.0276	0.0495	0.0156
	4	0.1697	0.1883	0.0356	0.0135	0.0406	0.0155

Table with some results of numerical simulations

$$\delta K_1^{rel} = \left(\left|K_1^{num} - K_1^{an}\right| / K_1^{an}\right), \quad \delta u^{max} = \max \left|\Delta u_i^{num} - \Delta u_i^{an}\right| / \Delta u_i^{an},$$

$$\delta u^{rms} = \sqrt{\sum \left(\left|\Delta u_i^{num} - \Delta u_i^{an}\right| / \Delta u_i^{an}\right)^2 / N}.$$

Case 1: penny-shaped crack under normal far-field stresses

N	$h/h^{\triangle}$	Constant approximation			Square root appr.		
		δK_1^{rel}	δu^{max}	δu^{rms}	δK_1^{rel}	δu^{max}	δu^{rms}
18	1	0.1364	0.2230	0.1697	0.0790	0.1740	0.1317
	2	0.1494	0.2670	0.2015	0.0388	0.1576	0.1296
220	1	0.2034	0.2489	0.1014	0.0786	0.1125	0.0550
	2	0.1870	0.2304	0.0947	0.0404	0.0791	0.0494
1010	1	0.2081	0.2473	0.0697	0.0701	0.0892	0.0350
	2	0.1793	0.2078	0.0577	0.0342	0.0543	0.0267
3932	1	0.2237	0.2444	0.0496	0.0650	0.0827	0.0235
	2	0.1757	0.1897	0.0380	0.0276	0.0495	0.0156
	4	0.1697	0.1883	0.0356	0.0135	0.0406	0.0155

Conclusions:

Case 1: penny-shaped crack under normal far-field stresses

N	$h/h^{\triangle}$	Constant approximation δK_1^{rel}	δu^{max}	δu^{rms}	Square root appr. δK_1^{rel}	δu^{max}	δu^{rms}
18	1	0.1364	0.2230	0.1697	0.0790	0.1740	0.1317
	2	0.1494	0.2670	0.2015	0.0388	0.1576	0.1296
220	1	0.2034	0.2489	0.1014	0.0786	0.1125	0.0550
	2	**0.1870**	0.2304	0.0947	**0.0404**	0.0791	0.0494
1010	1	0.2081	0.2473	0.0697	0.0701	0.0892	0.0350
	2	**0.1793**	0.2078	0.0577	**0.0342**	0.0543	0.0267
3932	1	0.2237	0.2444	0.0496	0.0650	0.0827	0.0235
	2	0.1757	0.1897	0.0380	0.0276	0.0495	0.0156
	4	**0.1697**	0.1883	0.0356	**0.0135**	0.0406	0.0155

1. Square-root approximation for edge elements brings significantly better accuracy of calculations. The biggest improvement can be observed for the K_1 .

Case 1: penny-shaped crack under normal far-field stresses

N	$h/h^{\triangle}$	Constant approximation δK_1^{rel}	δu^{max}	δu^{rms}	Square root appr. δK_1^{rel}	δu^{max}	δu^{rms}
18	1	0.1364	0.2230	0.1697	**0.0790**	0.1740	0.1317
	2	0.1494	0.2670	0.2015	**0.0388**	0.1576	0.1296
220	1	0.2034	0.2489	0.1014	**0.0786**	0.1125	0.0550
	2	0.1870	0.2304	0.0947	**0.0404**	0.0791	0.0494
1010	1	0.2081	0.2473	0.0697	**0.0701**	0.0892	0.0350
	2	0.1793	0.2078	0.0577	**0.0342**	0.0543	0.0267
3932	1	0.2237	0.2444	0.0496	**0.0650**	0.0827	0.0235
	2	0.1757	0.1897	0.0380	**0.0276**	0.0495	0.0156
	4	0.1697	0.1883	0.0356	**0.0135**	0.0406	0.0155

2. In case of the square-root approximation, results depended not only on the total number of elements N, but also on the boundary trapezoids height h.

Example: the penny-shaped crack in an infinite medium

Elements amount $N = 3932$

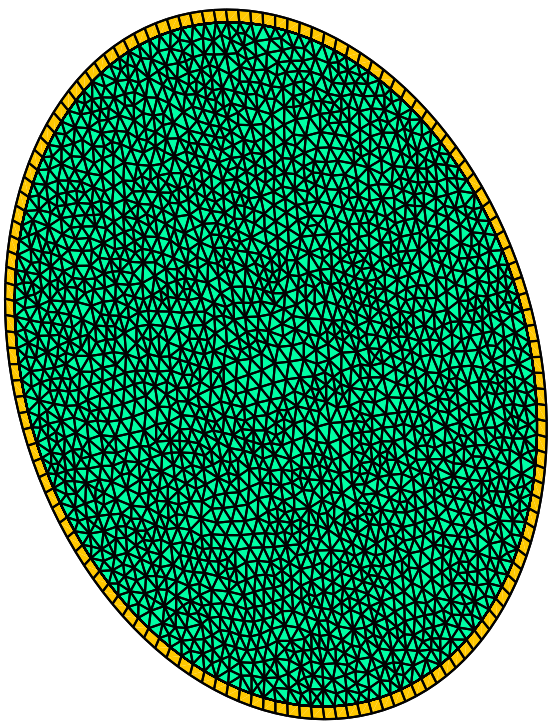

$h = h^{\triangle}$

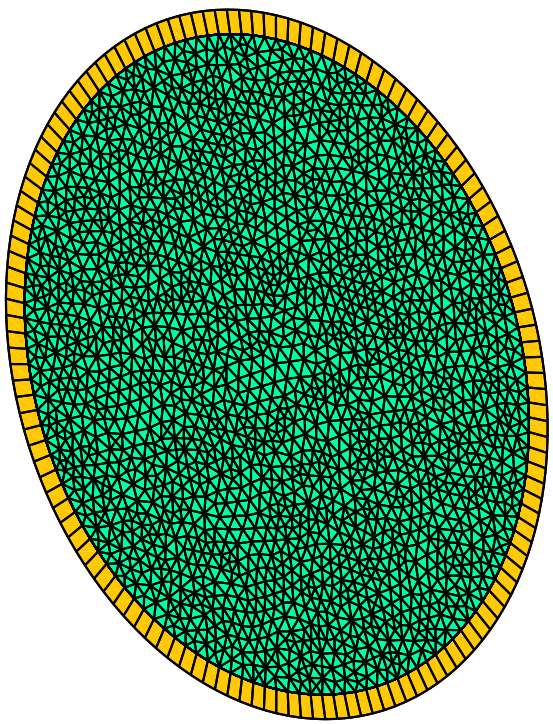

$h = 2h^{\triangle}$

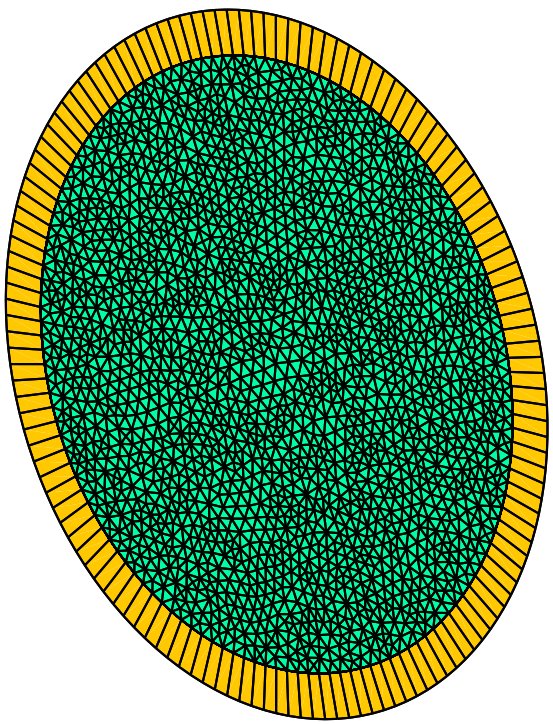

$h = 4h^{\triangle}$

Case 1: penny-shaped crack under normal far-field stresses

N	$h/h^{\triangle}$	Constant approximation δK_1^{rel}	δu^{max}	δu^{rms}	Square root appr. δK_1^{rel}	δu^{max}	δu^{rms}
18	1	0.1364	0.2230	0.1697	**0.0790**	0.1740	0.1317
	2	0.1494	0.2670	0.2015	**0.0388**	0.1576	0.1296
220	1	0.2034	0.2489	0.1014	**0.0786**	0.1125	0.0550
	2	0.1870	0.2304	0.0947	**0.0404**	0.0791	0.0494
1010	1	0.2081	0.2473	0.0697	**0.0701**	0.0892	0.0350
	2	0.1793	0.2078	0.0577	**0.0342**	0.0543	0.0267
3932	1	0.2237	0.2444	0.0496	**0.0650**	0.0827	0.0235
	2	0.1757	0.1897	0.0380	**0.0276**	0.0495	0.0156
	4	0.1697	0.1883	0.0356	**0.0135**	0.0406	0.0155

2. In case of the square-root approximation, results depend not only on the total number of elements N, but also on the boundary trapezoids height h.

Case 1: penny-shaped crack under normal far-field stresses

N	$h/h^{\triangle}$	Constant approximation δK_1^{rel}	δu^{max}	δu^{rms}	Square root appr. δK_1^{rel}	δu^{max}	δu^{rms}
18	1	0.1364	0.2230	0.1697	0.0790	0.1740	0.1317
	2	0.1494	0.2670	0.2015	0.0388	0.1576	0.1296
220	1	0.2034	0.2489	0.1014	0.0786	0.1125	0.0550
	2	0.1870	0.2304	0.0947	0.0404	0.0791	0.0494
1010	1	0.2081	0.2473	0.0697	0.0701	0.0892	0.0350
	2	0.1793	0.2078	0.0577	0.0342	0.0543	0.0267
3932	1	0.2237	0.2444	0.0496	0.0650	0.0827	0.0235
	2	0.1757	0.1897	0.0380	0.0276	0.0495	0.0156
	4	0.1697	0.1883	0.0356	0.0135	0.0406	0.0155

3. Influence coefficients evaluation time (*Intel i5-2540M*, 1 thread):
0.48s vs 0.63s (**24%** longer), **10.27s vs 11.36s** (**10%** longer),
147.94s vs 157.39s (**6%** longer).

Case 2: penny-shaped crack under shear far-field stresses

N	$h/h^{\triangle}$	δu^{max}	δu^{rms}	δK_2^{max}	δK_2^{rms}	δK_3^{max}	δK_3^{rms}
18	2	0.1625	0.1305	0.0455	0.0416	0.0536	0.0482
	2	0.2790	0.2018	0.1364	0.1294	0.1702	0.1604
220	2	0.0819	0.0490	0.0388	0.0358	0.0616	0.0458
	2	0.2454	0.0947	0.1774	0.1686	0.2517	0.2034
1010	2	0.0626	0.0273	0.0454	0.0303	0.0406	0.0366
	2	0.2148	0.0583	0.1923	0.1713	0.1988	0.1919
3932	4	0.0452	0.0161	0.0207	0.0126	0.0275	0.0150
	4	0.1997	0.0360	0.1685	0.1494	0.1807	0.1718

– constant approximation

– square-root approximation

Case 2: penny-shaped crack under shear far-field stresses

N	$h/h^{\triangle}$	δu^{max}	δu^{rms}	δK_2^{max}	δK_2^{rms}	δK_3^{max}	δK_3^{rms}
18	2	0.1625	0.1305	0.0455	0.0416	0.0536	0.0482
	2	0.2790	0.2018	0.1364	0.1294	0.1702	0.1604
220	2	**0.0819**	**0.0490**	0.0388	0.0358	0.0616	0.0458
	2	**0.2454**	**0.0947**	0.1774	0.1686	0.2517	0.2034
1010	2	0.0626	0.0273	**0.0454**	**0.0303**	0.0406	0.0366
	2	0.2148	0.0583	**0.1923**	**0.1713**	0.1988	0.1919
3932	4	0.0452	0.0161	0.0207	0.0126	**0.0275**	**0.0150**
	4	0.1997	0.0360	0.1685	0.1494	**0.1807**	**0.1718**

The same conclusions

Conclusions from 3D numerical examples

- the height of the square-root edge elements should be connected rather with surface geometry than other elements size;
- **square-root edge elements are not so computational-expensive and bring significantly better accuracy of calculations**.

Conclusions from 3D numerical examples

- the height of the square-root edge elements should be connected rather with surface geometry than other elements size;
- **square-root edge elements are not so computational-expensive and bring significantly better accuracy of calculations**.

Thank you for attention!